Human Molecular Genetics, 2009, Vol. 18, No. 23 **4629–4639**
doi:10.1093/hmg/ddp430
Advance Access published on September 10, 2009

GIGYF2 gene disruption in mice results in neurodegeneration and altered insulin-like growth factor signaling

Barbara Giovannone[1], William G. Tsiaras[1], Suzanne de la Monte[2], Jan Klysik[3], Corinne Lautier[1,†], Galina Karashchuk[1], Stefano Goldwurm[4] and Robert J. Smith[1,*]

[1]Division of Endocrinology and [2]Liver Research Center, Rhode Island Hospital, Alpert Medical School of Brown University, Providence, RI 02903, USA, [3]Department of Molecular Biology, Cell Biology and Biochemistry, Brown University, Providence, RI 02912, USA and [4]Parkinson Institute, Istituti Clinici di Perfezionamento, Milan 20126, Italy

Received June 19, 2009; Revised August 25, 2009; Accepted September 7, 2009

Grb10-Interacting GYF Protein 2 (GIGYF2) was initially identified through its interaction with Grb10, an adapter protein that binds activated IGF-I and insulin receptors. The *GIGYF2* gene maps to human chromosome 2q37 within a region linked to familial Parkinson's disease (PARK11 locus), and association of *GIGYF2* mutations with Parkinson's disease has been described in some but not other recent publications. This study investigated the consequences of *Gigyf2* gene disruption in mice. *Gigyf2* null mice undergo apparently normal embryonic development, but fail to feed and die within the first 2 post-natal days. Heterozygous *Gigyf2*$^{+/-}$ mice survive to adulthood with no evident metabolic or growth defects. At 12–15 months of age, the *Gigyf2*$^{+/-}$ mice begin to exhibit motor dysfunction manifested as decreased balance time on a rotating horizontal rod. This is associated with histopathological evidence of neurodegeneration and rare intracytoplasmic Lewy body-like inclusions in spinal anterior horn motor neurons. There are α-synuclein positive neuritic plaques in the brainstem and cerebellum, but no abnormalities in the substantia nigra. Primary cultured embryo fibroblasts from *Gigyf2* null mice exhibit decreased IGF-I-stimulated IGF-I receptor tyrosine phosphorylation and augmented ERK1/2 phosphorylation. These data provide further evidence for an important role of GIGYF2 in age-related neurodegeneration and IGF pathway signaling.

INTRODUCTION

Grb10-Interacting GYF Protein 2 (GIGYF2) was initially identified in our laboratory through yeast two-hybrid screening for binding partners of the Grb10 adapter protein (1). Grb10 is recruited to activated IGF-I and insulin receptors, as well as other receptor tyrosine kinases (2). Studies on *Grb10* null mice and cultured cells with siRNA knockdown of Grb10 strongly support a role for the endogenous Grb10 protein in negatively regulating IGF-I and insulin receptor signaling (3,4). GIGYF2 and the homologous GIGYF1 protein, which are encoded by distinct genes on human chromosomes 2 and 7, respectively, may be recruited to activated IGF-I and insulin receptors through binding to the N-terminus of Grb10, whereas the Grb10 C terminus interacts with the receptors. We have previously obtained evidence for IGF-I-stimulated GIGYF1 recruitment to Grb10, with resulting regulatory effects on IGF-I receptors (1). However, studies on GIGYF1 and GIGYF2 function have been limited by a propensity of these proteins to form toxic aggregates when over-expressed in cultured cells.

To gain insight into the potential functional role of GIGYF2, we examined human genome data for *GIGYF2* disease associations and noted that the *GIGYF2* gene is within the PARK11 Parkinson's disease linkage region on chromosome 2q37.1 (5). Since the IGFs and insulin have important effects in the central nervous system (6–8) and are potentially associated with Parkinson's disease (9–11),

*To whom correspondence should be addressed at: Division of Endocrinology, Rhode Island Hospital, One Hoppin Street, Suite 200, Providence, RI 02903, USA. Tel: +1 4014443420; Fax: +1 4014444921; Email: rsmith4@lifespan.org
†Present address: Universite Montpellier II, Montpellier, France.

we examined the *GIGYF2* gene for mutations in familial Parkinson's disease. Complete sequencing of the *GIGYF2* coding region in 254 patients with familial Parkinson's disease and 227 controls from distinct Italian and French populations demonstrated seven different missense mutations in 12 unrelated Parkinson's disease patients (4.8%), one mutation specific to the control population and several polymorphisms (12). A subsequent study on two Asian populations described distinct non-synonymous *GIGYF2* variants and confirmed a significant increase in these variants in Parkinson's disease patients compared with healthy controls (13). However, multiple other reports on additional populations with a mix of sporadic and familial Parkinson's disease have not found the association of *GIGYF2* mutations with Parkinson's disease (14–19) or linkage at the PARK11 site via the *GIGYF2* gene (20). Thus, there is uncertainty about the role of GIGYF2 as a contributory factor in Parkinson's disease (21).

We here report the generation of a mouse *Gigyf2* gene disruption model as an independent approach to further investigating GIGYF2 function. The *Gigyf2* null mice exhibit early post-natal lethality. Heterozygous *Gigyf2*$^{+/-}$ mice initially survive and grow normally, but develop adult-onset neurodegeneration. Primary cultured fibroblasts from embryonic *Gigyf2* null mice manifest IGF-I receptor signaling abnormalities.

RESULTS

Gigyf2 gene disruption

A gene trap strategy was used to generate a mouse line with inactivation of the *Gigyf2* gene. For this purpose, mouse embryonic stem cells were obtained with a gene trap construct composed of a splice acceptor, beta-geo cassette and polyadenylation sequence inserted into the proximal coding region of the *Gigyf2* gene (Bay Genomics, http://baygenomics.ucsf.edu). We mapped the insertion point of the construct within the 5 kb intron between *Gigyf2* exons 4 and 5 using intronic and gene trap PCR primer pairs (Fig. 1A). This predicted a truncated transcript with deletion of 23 of the total 27 exons of *Gigyf2*. Genotyping of mouse colony progeny obtained from crosses of parental mice heterozygous for the gene trap insert demonstrated E17.5 embryos with each of the three expected genotypes (Fig. 1B). Northern blotting analysis of total RNA extracts from primary mouse embryonic fibroblast (MEF) cultures derived from E12.5 embryos using a probe corresponding to the first 4 exons of *Gigyf2* is shown in Figure 1C. A single 7 kb GIGYF2 mRNA band was observed in the wild-type +/+ MEFs, a smaller 6 kb band corresponding to the reduced size expected for the truncated gene trap-containing transcript in the homozygous *Gigyf2*$^{-/-}$ MEFs, and both bands in MEFs from heterozygous +/− progeny. Similar data were obtained using total RNA extracts from whole E17.5 mouse embryos (data not shown). Northern blotting with a *Gigyf2* cDNA probe corresponding to sequence downstream from the gene trap insert demonstrated a single band in the wild-type +/+ MEFs, a lower intensity single band of the same size in heterozygous +/− MEFs, and no hybridizing band in the −/− MEFs (Fig. 1D). This confirmed the absence of transcribed full-length mRNA sequence downstream from the gene trap. The failure to detect smaller bands on these blots further indicated that bypassing of the gene trap by alternative splicing or alternative start codons was not occurring. Northern blotting with a probe specific for the homologous *Gigyf1* gene (1) demonstrated a single band of equal intensity in mice of all three genotypes (Fig. 1E), indicating a lack of upregulation of *Gigyf1* mRNA in response to loss of *Gigyf2* expression.

Immunoblotting of total cell lysates with an affinity-purified GIGYF2 anti-peptide antibody confirmed the presence of a GIGYF2 band at 180 kDa in wild-type MEFs (Fig. 1F). This band was confirmed to correspond to full-length GIGYF2 based on its recognition by both N-terminal and C-terminal anti-GIGYF2 peptide antibodies (data not shown). The GIGYF2 protein was undetectable in −/− MEFs, and a 180 kDa band of ∼50% lower intensity compared with the control cells was present in the +/− heterozygotes. A similar partial decrease of GIGYF2 protein in heterozygotes and absence of expression in −/− animals was demonstrated by immunoblotting of extracts from whole E14.5 embryos (Fig. 1G). Immunoblotting of whole embryo extracts (data not shown) and MEF lysates (Fig. 1H) with GIGYF1 antibody identified a dominant band of the expected 150 kDa size for the full-length GIGYF1 protein, which was present at equal intensity in all three genotypes. Thus, consistent with the northern blotting data, there is a partial (∼50%) decrease in abundance of the GIGYF2 protein in heterozygotes and a complete absence of detectable GIGYF2 protein in the −/− homozygotes. The homologous GIGYF1 protein is expressed and not changed in abundance in control versus GIGYF2-deficient mice.

Effects of *Gigyf2* gene disruption on embryonic and post-natal survival

Analysis of genotype frequency in late gestation embryos (E17.5–18.5) from heterozygous matings demonstrated the predicted Mendelian genotype distribution, consistent with the generation and survival of heterozygous and homozygous *Gigyf2* gene-disrupted mice equivalent to the wild-type (Table 1). However, we observed that a substantial number of newborn animals from the heterozygous matings did not survive beyond the first post-natal day. When both surviving and non-surviving animals were collected during the first day after birth and analyzed, the cumulative genotype frequencies were close to the Mendelian ratio observed for the late gestation embryos (Table 1). Progeny deaths were limited almost entirely to the first post-natal day and specifically occurred in the *Gigyf2* null (−/−) newborns. The modest (25%) decrease in the number of *Gigyf2*$^{-/-}$ compared with wild-type +/+ newborn mice observed at the first post-natal day (Table 1) likely reflected the failure to recover some non-surviving −/− animals as a consequence of post-mortem maternal cannibalism. At the time of weaning (day P21), genotyping revealed the predicted 2:1 ratio of *Gigyf2*$^{+/-}$ to +/+ animals, but a marked decrease in the *Gigyf2* null (−/−) genotype, consistent with ∼85% lethality of the *Gigyf2* null mice during the first post-natal day (Table 1). The *Gigyf2* heterozygotes were indistinguishable from the

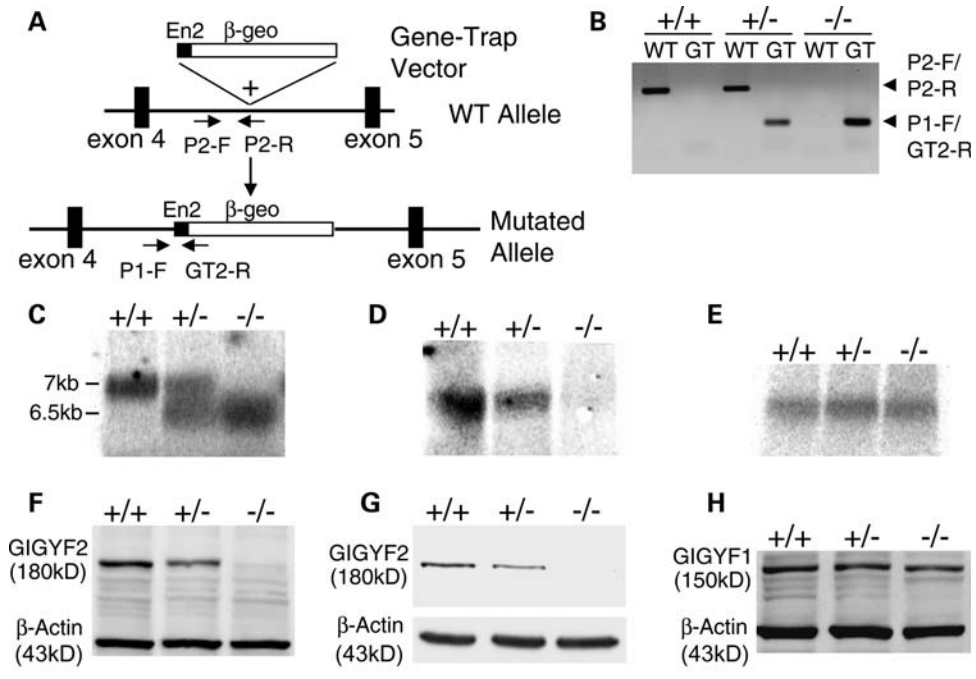

Figure 1. Gene trap disruption of the *Gigyf2* gene locus. (**A**) Schematic representation of the partial genomic structure of the mouse *Gigyf2* gene before and after the gene trap integration. (**B**) PCR analysis of DNA from E17.5 embryos obtained in crosses of $Gigyf2^{+/-}$ mice. Primers P2-F and P2-R were used to amplify a 639 bp fragment (WT allele), whereas primers P1-F and GT2-R were used to amplify a 290 bp fragment (mutated allele). (**C**) Northern blot of total RNA from primary MEFs isolated from $Gigyf2^{+/+}$, $+/-$, $-/-$ mice using a 450 bp probe of the first 4 exons of the mouse *Gigyf2* gene upstream from the gene trap. (**D**) Similar northern blot using a C terminus probe. (**E**) Northern blot of total RNA from primary MEFs isolated from $Gigyf2^{+/+}$, $+/-$, $-/-$ mice using a 450 bp probe corresponding to the mouse *Gigyf1* gene. (**F**) Immunoblot of total proteins from primary MEFs isolated from $Gigyf2^{+/+}$, $+/-$, $-/-$ mice using a GIGYF2 antibody and β-actin antibody to control for loading. (**G**) Similar immunoblot of extracts from E14.5 whole embryos. (**H**) Immunoblot of total proteins from $Gigyf2^{+/+}$, $+/-$, $-/-$ MEFs using a GIGYF1 antibody.

Table 1. Progeny from $Gigyf2^{+/-}$ matings

Genotype	E17.5–18.5		P1		P21	
	No.	%	No.	%	No.	%
$+/+$	23	25.6	12	27.9	87	31.9
$+/-$	47	52.2	22	51.2	172	63.0
$-/-$	20	22.2	9	20.9	14	5.1

E, embryonic day; P, post-natal day. Data represent number of animals identified with each genotype and percent of each genotype at the indicated ages.

wild-type animals in growth curves and adult size and weight, and appeared to have normal fertility. There were not enough surviving $Gigyf2^{-/-}$ mice to define their growth characteristics.

Examination of fetal animals of all three genotypes in late gestation (E17.5) revealed no differences among the wild-type, heterozygous and *Gigyf2* null mice in gross appearance, linear growth or body weight (Fig. 2A–C). In contrast, during the first post-natal day, crown-rump length and body weight were significantly lower in *Gigyf2* null ($-/-$) animals (Fig. 2D–F). This correlated with a marked decrease in size of the gastric milk spot in the *Gigyf2* null mice compared with wild-type and heterozygotes (Fig. 2D and G), indicating a failure of the *Gigyf2* null newborns to feed. The rapid loss of weight and less marked decrease in crown-rump length likely were secondary to dehydration, and the magnitude of the feeding deficit appeared adequate to explain the observed mortality rate. The newborn *Gigyf2* null mice had normal motility based on timed self-righting capacity and detailed anatomic and histological examination of P1 mice showed no abnormalities in nasal, oropharyngeal or gastrointestinal structures (data not shown). The *Gigyf2* null mice also were not cyanotic and had no detectable pulmonary or cardiac abnormalities. The mean body weight and milk spot size of animals heterozygous for *Gigyf2* gene disruption were slightly lower than wild-type controls (Fig. 2F–G). Although these differences were not statistically significant with the number of animals studied, they suggest a possible intermediate phenotype with partial loss of the GIGYF2 protein.

Tissue and cellular expression of *Gigyf2*

The gene trap construct contains a β-galactosidase sequence under control of the endogenous *Gigyf2* promoter. By staining sections of $Gigyf2^{+/-}$ and $-/-$ embryos with X-gal, it thus is possible to determine the tissue and cellular sites of *Gigyf2* promoter activity as a surrogate for *Gigyf2* gene expression at different stages of development. As shown in Figure 3A, *Gigyf2* is broadly expressed in embryonic mouse tissues, including strong expression in the central nervous system. X-gal staining is more intense in $-/-$ compared with $+/-$

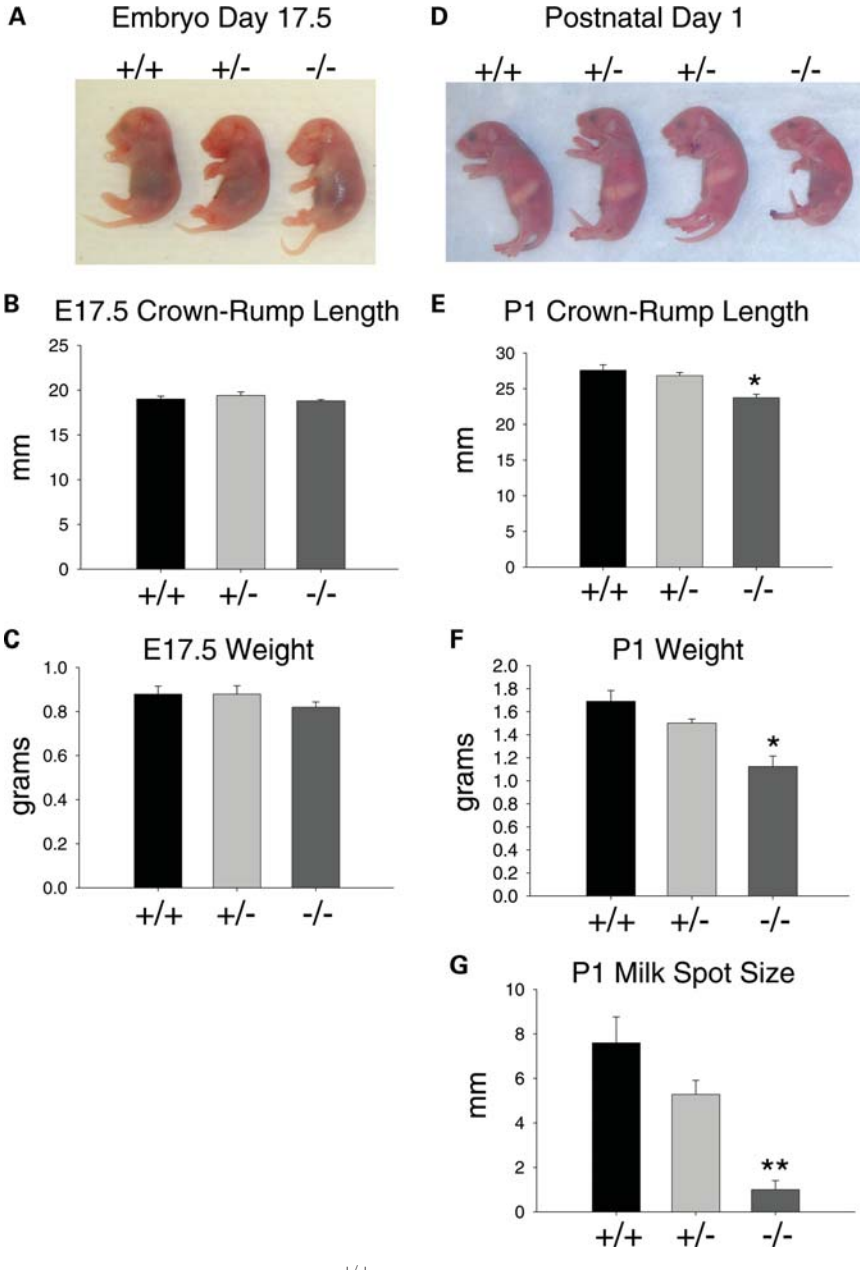

Figure 2. Phenotype of *Gigyf2* knockout mice. (**A**–**F**) Size of *Gigyf2*$^{+/+}$, $+/-$ and $-/-$ mice was assessed at embryonic day 17.5 (E17.5) and post-natal day 1 (P1) by measuring crown-rump length and weight. (**G**) Milk spot size in P0–1 mice was assessed as length across the longest diagonal. For E17.5 mice, $+/+$ $n = 5$, $+/-$ $n = 5$ and $-/-$ $n = 7$; for P1 mice, $+/+$ $n = 5$, $+/-$ $n = 18$ and $-/-$ $n = 4$. Plotted data are means $\pm$ SD, subjected to a two-tailed *t*-test for comparison of $+/-$ and $-/-$ mice to $+/+$ ($^{*}P < 0.005$; $^{**}P < 0.002$).

mice, consistent with the presence of two versus one copy of the reporter allele, respectively. Wild-type mice had absent X-gal staining (data not shown). *Gigyf2* gene promoter activity was observed throughout the CNS in adult *Gigyf2*$^{-/-}$ mice (Fig. 3Ba). Animals of this genotype were used, since they have a strong *Gigyf2* promoter-driven β-galactosidase signal, and they were confirmed to have no histological changes from wild-type or *Gigyf2*$^{+/-}$ mice by Luxol Fast Blue H&E staining. *Gigyf2* expression was noted to be especially marked in cerebellar Purkinje cells, the pons and the choroid plexus (Fig. 3Bb–e). High intensity staining was evident in both neuronal and glial cells in multiple brain regions (Fig. 3C).

Motor dysfunction in heterozygous *Gigyf2*$^{+/-}$ mice

Given the potential association of the *GIGYF2* gene with human Parkinson's disease (12), which most frequently has onset in adulthood and increases in prevalence with advancing age, we examined neurological function in post-natal *Gigyf2*$^{+/-}$ mice up to 18 months of age. An adequate number of surviving $-/-$ mice were not available for

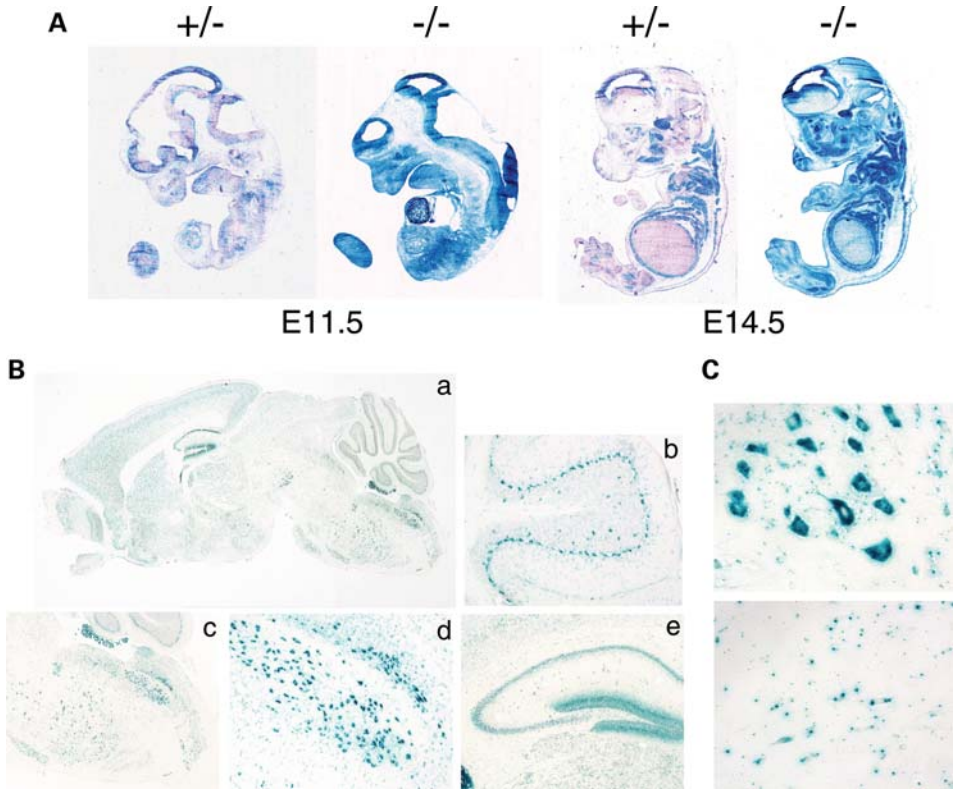

Figure 3. *Gigyf2* promoter activity in knockout mice. (**A**) Whole mount embryos of different stages expressing β-galactosidase from the *Gigyf2* promoter. (**B**) β-Galactosidase staining of sections of *Gigyf2*$^{-/-}$ mouse brain: (a) sagittal section (×1) of full brain, (b) cerebellar region (×10), (c) pons region (×4), (d) pons region (×10) and (e) coronal section of hippocampal region (×4). (**C**) Cell type expression of β-galactosidase in *Gigyf2*$^{-/-}$ mouse brain: neurons (top panel) and glia (bottom panel).

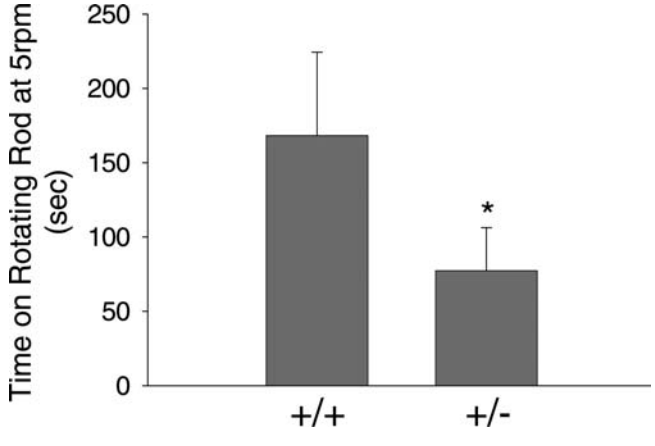

Figure 4. Motor dysfunction in *Gigyf2* heterozygous mice. Rotating rod performance of 15-month-old male *Gigyf2*$^{+/-}$ mice compared with age-matched *Gigyf2*$^{+/+}$ controls. Six-independent trials were conducted in which time on a 5 r.p.m. rotating rod was recorded for all mice (+/+ $n = 4$, +/− $n = 10$). Data plotted are means ± SD, subjected to a one-tailed *t*-test for comparison between +/+ and +/− mice ($^{*}P < 0.05$).

investigation of neurological function or histopathology (see below). Abnormalities were not evident in the heterozygous *Gigyf2*$^{+/-}$ animals until ∼12 months of age, at which point mild truncal and hindlimb motor dysfunction became apparent as an exaggerated splaying of the hindlimbs with delayed positional correction when animals were dropped 15 cm onto a flat surface. This abnormal motor response was present in ∼50% of 12-month-old *Gigyf2*$^{+/-}$ mice and absent from wild-type (*Gigyf2*$^{+/+}$) littermates, as assessed by an investigator unaware of the genotype of individual animals. As a more quantitative test, balance performance on a rotating horizontal rod then was determined. As shown for 15-month-old mice in Figure 4, animals with inactivation of one *Gigyf2* gene allele exhibited an ∼50% decrease in staying time on a rod rotating at 5 r.p.m. compared with wild-type controls ($P < 0.05$).

Neurodegeneration in *Gigyf2*$^{+/-}$ mice

Histological sections were examined from the brain and spinal cord of 15-month-old *Gigyf2*$^{+/-}$ and control (+/+) mice. In Luxol Fast Blue H&E stained sections, there was evidence of motor neuron degeneration at multiple spinal cord levels in *Gigyf2*$^{+/-}$ mice. Specific pathological findings included eosinophilic degeneration with nuclear pyknosis, axonal swelling and rare inclusion body-like structures affecting predominantly large pyramidal neurons in the ventral horns of the spinal cord (Fig. 5A). Histomorphometric quantitation of neuronal and glial cell number in lumbar region spinal cord sections confirmed a significant decrease in the neuronal/glial cell ratio (Fig. 5B). This was associated with a non-significant

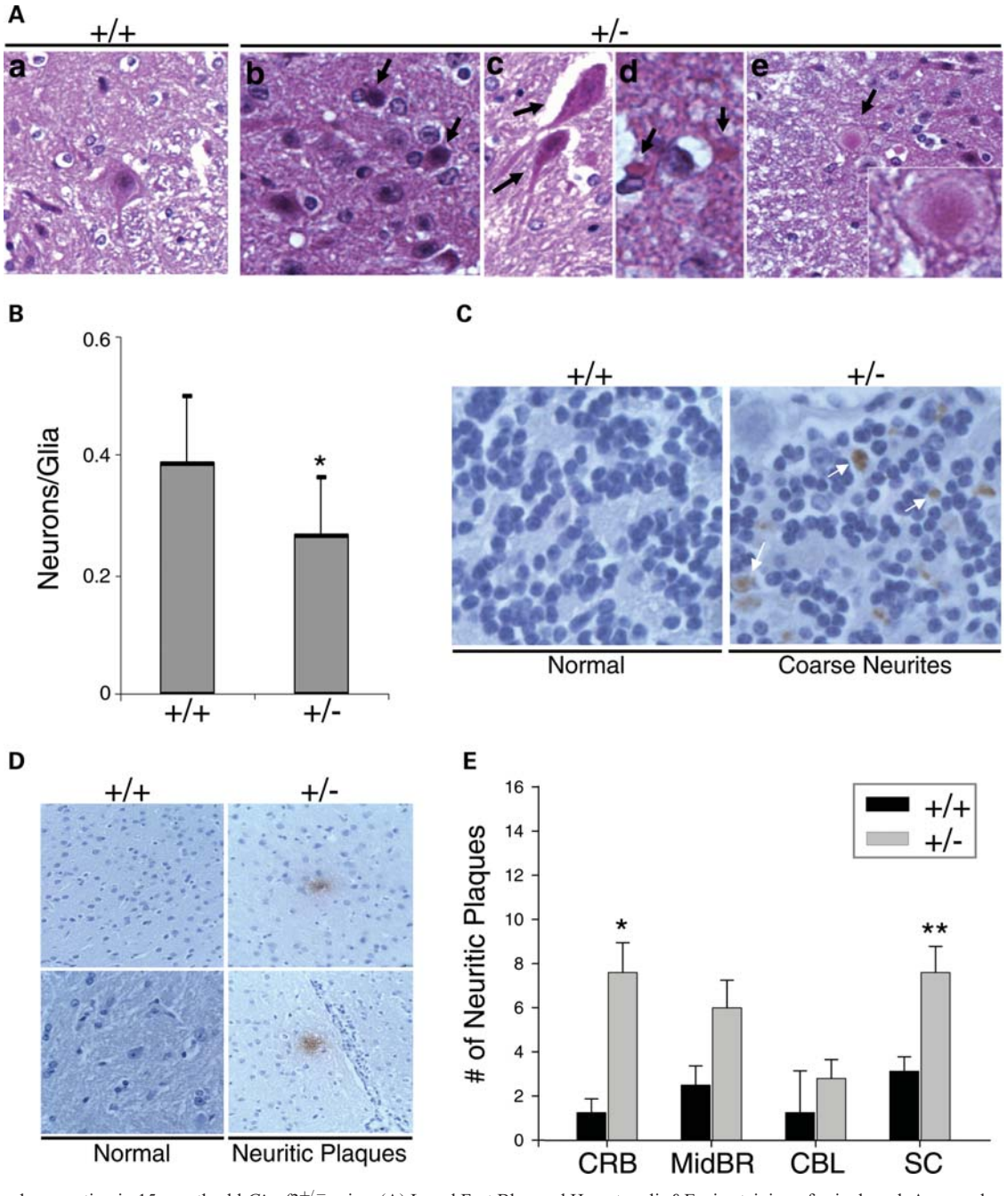

Figure 5. Neurodegeneration in 15-month-old *Gigyf2*$^{+/-}$ mice. (**A**) Luxol Fast Blue and Hematoxylin&Eosin staining of spinal cord. Arrows show eosinophylic (hypoxic-appearing) motor neurons (b), swollen axons (c and d) and inclusion body-like structures (e and inset window) in *Gigyf2*$^{+/-}$ mice compared with a healthy motor neuron in a *Gigyf2*$^{+/+}$ control animal (a). (**B**) Ratio of neurons and glial cells per unit of surface area counted from 2 to 3 independent sections from sacral and lumbar regions of spinal cords from *Gigyf2*$^{+/+}$ ($n = 4$) and *Gigyf2*$^{+/-}$ ($n = 4$) mice. Data plotted are means $\pm$ SD, subjected to a Mann–Whitney rank sum test for comparison between +/+ and +/− animals ($^{*}P < 0.05$). (**C**) α-Synuclein staining of cerebellar granule cell layer. Arrows indicate examples of coarse neurites in a *Gigyf2*$^{+/-}$ mouse, which are absent in the age-matched *Gigyf2*$^{+/+}$ mouse. (**D**) Immunohistochemical staining of cerebral cortex (top panels) and midbrain (bottom panels) with an α-synuclein antibody shows neuritic plaques in a *Gigyf2*$^{+/-}$ compared with an age-matched +/+ mouse. (**E**) Number of neuritic plaques per section across several regions of brain (CRB, cerebrum, MidBR, midbrain, CBL, cerebellum and SC, spinal cord). Data are means $\pm$ SD from +/+ $n = 4$ and +/− $n = 10$, subjected to a two-tailed *t*-test for comparison between +/+ and +/− groups ($^{*}P < 0.02$ and $^{**}P < 0.05$).

decrease in neuron number and non-significant increase in glial cells, when assessed independently.

There were no overt neuronal or glial cellular abnormalities on Luxol Fast Blue H&E staining in the cerebrum, midbrain or cerebellum (data not shown), but immunostaining with α-synuclein antibody yielded additional evidence of neuronal abnormalities and neurodegeneration in these brain regions. This included α-synuclein positive, coarse neurites in the cerebellar granule cell layer of the *Gigyf2*$^{+/-}$ mice, but not in age-matched (*Gigyf2*$^{+/+}$) controls (Fig. 5C). Increased

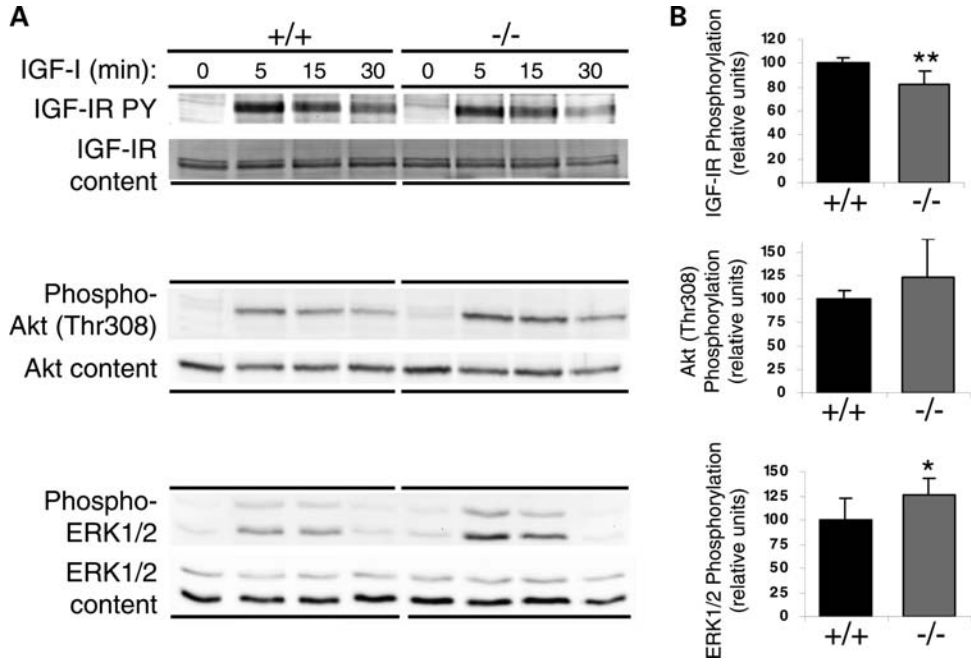

Figure 6. IGF-I-stimulated cell signaling in *Gigyf2*$^{-/-}$ mouse embryonic fibroblasts. Passage 4 MEFs derived from *Gigyf2*$^{+/+}$ and $-/-$ mice were treated with IGF-I for the length of time indicated and total cell lysates were used for immunoblotting. (**A**) IGF-I receptor (IGF-IR), Akt and ERK1/2 activation were assessed in two littermate matched pairs of $+/+$ and $-/-$ MEFs using phospho-specific antibodies (representative blot from a single pair shown). (**B**) Six littermate-matched pairs of $+/+$ and $-/-$ MEFs from three-independent litters were treated with IGF-I for 0 or 5 min and analyzed as described in (A). Phosphorylation was quantified by densitometry and normalized to protein content. Fold increase in phosphorylation at 5 min compared with basal was determined for each cell line. Relative units were obtained by normalizing each fold increase to a mean $+/+$ value of 100. Data plotted are means $\pm$ SD. The data were subjected to two-tailed *t*-test analysis for comparison between $+/+$ and $-/-$ MEFs ($^{*}P < 0.02$, $^{**}P < 0.002$).

numbers of α-synuclein-positive neurites were diffusely present throughout the brain and spinal cord of *Gigyf2*$^{+/-}$ animals in comparison with controls (Fig. 5D). Quantitative histomorphometry by an observer unaware of the genotypes of individual animals confirmed a statistically significant increase in α-synuclein-positive neuritic plaques in *Gigyf2*$^{+/-}$ cerebrum and spinal cord (Fig. 5E). The mean number of plaques also was higher in midbrain and cerebellum of *Gigyf2*$^{+/-}$ versus control animals, but this did not reach statistical significance. The total brain plaques per section and also the number of plaques per section in specific brain regions (midbrain, cerebellum or cerebrum) in the individual *Gigyf2*$^{+/-}$ animals correlated inversely with balance time on the horizontal rotating rod. Linear regression analysis of total brain plaques per section versus time on the rotating rod in seconds for the 10 heterozygous knockout mice demonstrated a slope of -0.0269 ($P < 0.001$).

Neuronal loss was not evident in the substantia nigra as assessed by Luxol Fast Blue H&E or anti-tyrosine hydroxylase immunofluorescent staining (data not shown). There also were no abnormalities evident in brain or spinal cord sections immunostained with antibodies to glial fibrillary acid protein (GFAP) or ubiquitin.

IGF signaling in MEFs from *Gigyf2* null mice

GIGYF2 was initially identified in a yeast two-hybrid screen as a binding partner for the Grb10 adapter protein (1). Since Grb10 is recruited to activated IGF-I and insulin receptors, and it negatively regulates IGF and insulin signaling (3,4), we considered the potential role of decreased GIGYF2 levels in modifying the actions of these hormones. As evident in Figure 2 A–C, both the *Gigyf2*$^{+/-}$ heterozygotes and the *Gigyf*$^{-/-}$ mice exhibited normal embryonic and fetal growth. When examined post-natally, the adult *Gigyf2*$^{+/-}$ heterozygotes and the small number of surviving *Gigyf2*$^{-/-}$ mice were indistinguishable from wild-type littermates in length, body weight and blood glucose levels (data not shown). Abnormalities in growth and glucose levels were not evident in the few *Gigyf2*$^{-/-}$ mice that survived to adulthood, but adequate numbers were not available to formally assess these animals.

As an initial approach to further examining the effects of GIGYF2 on cell survival, we determined the percentage of randomly cycling primary MEFs from *Gigyf2*$^{+/+}$ and $-/-$ mice in S-phase by flow cytometry in the absence or presence of the DNA cross-linking agent etoposide under serum-stimulated conditions. The percentage of cells in S-phase under control conditions was similar for *Gigyf2*$^{+/+}$ and $-/-$ MEFs (28.7 ± 4.1 versus 30.3 ± 3.5, respectively, $n = 3$). Etoposide resulted in a marked (80%) decrease in the number of *Gigyf2*$^{+/+}$ cells in S-phase, consistent with the expected decrease in S-phase entry following DNA damage. There was a significantly higher percentage of *Gigyf2*$^{-/-}$ compared with $+/+$ cells in S-phase after etoposide (12.1% of $-/-$ in S-phase versus 5.6% of $+/+$ in S-phase, $P = 0.026$). These findings suggest dysregulation of cell cycle control with *Gigyf2* gene dysruption.

To more specifically examine the effects of decreased GIGYF2 protein on receptor signaling, IGF-I stimulation of IGF-I receptor tyrosine phosphorylation and the activation of the downstream signaling intermediates Akt and ERK1/2 were assessed in multiple isolates of primary MEFs from *Gigyf2*$^{+/+}$ and −/− mice. IGF-I receptor abundance was similar in the wild-type and *Gigyf2* null MEFs based on immunoblotting with receptor antibody, and IGF-I-stimulated receptor tyrosine phosphorylation as assessed by phospho-specific antibody in a time-dependent manner, with a maximum effect at 5 min (Fig. 6A). Quantitation at the 5 min time point in multiple MEF isolates confirmed a modest but statistically significant (∼25%) lower level of IGF-I-stimulated receptor tyrosine phosphorylation in the *Gigyf2* null cells compared with wild-type (Fig. 6B). Determination of Akt and ERK1/2 activation by immunoblotting of the same cell extracts with phospho-specific antibodies for each of these intracellular signaling proteins demonstrated a similar time course of activation by IGF-I with a maximum effect at 5 min (Fig. 6A). In contrast with the inhibition of IGF-I-stimulated receptor tyrosine phosphorylation in *Gigyf2* null MEFs, disruption of the *Gigyf2* gene resulted in a modest but significant increase in IGF-I stimulation of ERK1/2 (25%, $P < 0.02$) (Fig. 6B). There was a similar magnitude increase in IGF-I-stimulated Akt activation in the *Gigyf2* null MEFs, with larger variation in the level of phospho-Akt such that the increase was not statistically significant (Fig. 6B). These experiments provide evidence of a role for the GIGYF2 protein in the regulation of IGF-I receptor signaling. The decrease in IGF-I-stimulated receptor tyrosine phosphorylation and oppositely directed augmentation of IGF-I effect on ERK1/2 and possibly Akt activation in *Gigyf2* null MEFs is similar to the previously described effects of knockdown of the GIGYF2 binding partner, Grb10, in cultured fibroblasts (4).

DISCUSSION

This report describes an adult onset neurodegeneration phenotype in a mouse model of *Gigyf2* gene disruption. *Gigyf2* null mice had normal intrauterine growth, and there were no evident anatomic or histological abnormalities in full-term fetuses. However, newborn mice lacking GIGYF2 failed to feed, as evidenced by reduced gastric milk spots together with post-natal weight loss, and exhibited 85% mortality during the first day after birth. The homologous GIGYF1 protein, which is encoded by a distinct gene, was shown to be present but not up-regulated in the mice with *Gigyf2* gene disruption, and the lethal phenotype confirmed a lack of compensation for GIGYF2 function by GIGYF1.

The *Gigyf2* null animals had normal self-righting behavior, an absence of gross abnormalities in motility, normal induced suckling movements and no apparent defects in oropharyngeal or nasal structures that might explain the failure to feed. Previous studies from other groups have demonstrated a phenotype in mice with olfactory dysfunction similar to the *Gigyf2* null mice, including absent gastric milk spot, perinatal weight loss and high early mortality (22,23). Olfactory sensory map development is regulated by IGF-I (24), and defects in olfaction frequently develop early in the course of both Parkinson's disease and Alzheimer's disease (25). Investigation of olfactory system development and function in *Gigyf2* null mice would be of interest in future studies using techniques such as electrophysiological olfactory neuronal mapping (22,26).

Heterozygous mice with gene trap disruption of a single *Gigyf2* allele have an ∼50% decrease in the abundance of GIGYF2 mRNA and protein. The *Gigyf2*$^{+/-}$ mice survive embryonic life at the expected Mendelian ratio and are indistinguishable from *Gigyf2*$^{+/+}$ littermate controls in growth and development. Neurological deficits were not evident in growing or young adult mice. However, by 15 months of age, ∼50% of the *Gigyf2*$^{+/-}$ mice developed motor dysfunction, which was quantifiable as a 50% decrease in balance time on a horizontal rotating rod compared with wild-type controls.

Histological examination of 15-month-old *Gigyf2*$^{+/-}$ animals demonstrated central nervous system abnormalities that included coarse neurites in the cerebellar granule cell layer, α-synuclein positive neuritic plaques in the brain and spinal cord, scattered inclusion body-like structures and spinal cord motor neurons with eosinophilic-stained cell bodies and swollen axons. Neurons appeared grossly normal in the substantia nigra, and nigral abnormalities were not evident by α-synuclein or tyrosine hydroxylase immunostaining. Quantitative histomorphometry confirmed a significant increase in α-synuclein positive neurites in the cerebrum and spinal cord, and the number of total brain α-synuclein plaques in individual mice correlates with the extent of decrease in motor function. These findings are consistent with a neurodegenerative process in the *Gigyf2*$^{+/-}$ mice that either has its onset in adulthood, or progresses to detectable levels with aging. Although we confirmed a statistically significant decrease in the ratio of neurons to glial cells in the lumbar spinal cord, this was associated with a non-significant decrease in neuron number and increase in glial cell number per cross-sectional area. It thus is possible that decreased GIGYF2 may affect glial as well as neuronal cell populations. Consistent with the observed effects of *Gigyf2* gene disruption on cells in the cerebrum, midbrain, cerebellum and spinal cord, GIGYF2 mRNA is expressed at multiple sites throughout the central nervous system.

Although the *Gigyf2*$^{+/-}$ mice manifest motor dysfunction, they do not have other features typical for human Parkinson's disease, such as an evident tremor or neuronal loss in the substantia nigra. Other mouse models with disruption of genes with established links to Parkinson's disease also do not fully recapitulate the functional and pathological features of the human disorder. For example, disruption of the *Parkin* or *DJ-1* genes in mice results in neurodegeneration and motor function deficits, but these animals do not have cellular deficits in the nigrostriatal dopaminergic pathway (27–29). In contrast, transgenic mice over-expressing human *SNCA* have dopaminergic neuronal loss, especially when the transgene is specifically driven by a dopaminergic neuron-targeted tyrosine hydroxylase promoter (30). The observation of inclusion body-like structures suggestive of Lewy bodies in the brain and spinal cord is a distinct feature of the *Gigyf2*$^{+/-}$ mice, which has not been described in other mouse models with disruption of Parkinson's disease-associated genes. When an

adequate antibody probe becomes available, it will be important to determine if GIGYF2 is present in the α-synuclein positive inclusion bodies or neuritic plaques in the *Gigyf2*$^{+/-}$ mice. The anti-GIGYF2 antibodies that we have generated are effective for immunoblotting, but do not have adequate specificity for the assessment of GIGYF2 by immunohistochemistry.

We previously demonstrated in a yeast two-hybrid assay that the protein encoded by the *GIGYF2* gene is a binding partner for the Grb10 adapter protein (1). Grb10 is known to interact with intracellular domains of activated insulin and IGF-I receptors and negatively regulate insulin and IGF signaling (3,4). As a protein that may be interactive with receptors via the adapter function of Grb10, GIGYF2 is of interest as a potential mediator or regulator of hormone signaling. We therefore compared IGF-I signaling in cultured MEFs from *Gigyf2*$^{-/-}$ and control +/+ mice. This demonstrated a modest but significant decrease in IGF-I-stimulated receptor phosphorylation in *Gigyf2*$^{-/-}$ cells, with no change in receptor abundance in comparison with control cells. In contrast, there was a significant increase in IGF-I-stimulated ERK1/2 phosphorylation and a suggestive, non-significant increase in Akt phosphorylation in the *Gigyf2* null cells. We also observed increased numbers of randomly cycling *Gigyf2* null MEFs in S-phase following treatment with the DNA cross-linking agent etoposide. In future studies, it will be of interest to determine whether this results from dysregulation of IGF-I effects on cell cycle control, which might increase susceptibility to apoptosis.

In previous work, Grb10 knockdown in cultured fibroblasts resulted in a similar decrease in IGF-I receptor tyrosine phosphorylation and an increase in downstream signaling from the IGF-I receptor (4), as well as similar effects on insulin receptor tyrosine phosphorylation and its downstream signaling (3). Recruitment of endogenous Grb10 to activated IGF-I and insulin receptors is thought to block receptor dephosphorylation by phosphoprotein phosphatases and simultaneously inhibit downstream signals that are generated by the tyrosine kinase activity of the receptors (4). In future studies, it will be important to determine whether the observed effects of GIGYF2 on IGF-I receptor phosphorylation and signaling are mediated via a GIGYF2-receptor protein complex with Grb10 functioning as a linker or by GIGYF2 modulating the capacity of Grb10 to bind the receptors.

The identification of *GIGYF2* as a gene linked to neurodegeneration as well as IGF-I and insulin signaling is of interest because of emerging evidence for a role of both of these hormones in human neurodegenerative disorders, including Parkinson's disease (6,7,31,32). IGF-I stimulates brain growth *in vivo* (33), promotes neuronal proliferation and differentiation and inhibits neuronal apoptosis (8). IGF-I receptors are abundantly expressed in the midbrain, and IGF-I has specifically been shown to decrease dopamine-induced cell death in rat cerebellar cell cultures and a human neuroblastoma cell line (9). Insulin receptors are abundant at various sites in the central nervous system, including the substantia nigra and basal ganglia (34). A role for diminished insulin signaling in Alzheimer's disease has been proposed (32), and a selective decrease in insulin receptor mRNA and protein in the substantia nigra in Parkinson's disease has been described (10). Diabetes has been associated with increased risk of Alzheimer's disease (35,36), and an approximately two-fold increased risk of Parkinson's disease in patients with type 2 diabetes mellitus (11). Further studies will be needed to determine whether the *GIGYF2* gene is functionally linked to Parkinson's disease. More data on of the molecular function of the GIGYF2 protein may provide insight into mechanisms through which mutations or altered expression of GIGYF2 result in neurodegeneration.

MATERIALS AND METHODS

Generation of *Gigyf2* gene-disrupted mice

Mice with disruption of the *Gigyf2* gene on a mixed C57BL/6-Tyr$^{c\text{-}Brd}$/129Ola background were generated using *Gigyf2* gene trap 129Ola ES cells (XH076) from Bay Genomics (UC San Francisco). The gene trap integration site in the *Gigyf2* gene was defined by sequencing of PCR products yielding a 290 bp fragment from intron 4 of the gene trap-containing *Gigyf2* gene (P1-F: 5′-GGGTGCCAAACTC AGTCCATTC-3′ and GT2-R: 5′-CGTGTCCTACAACAC ACACTCCAACC-3′) and a 639 bp fragment from the wild-type allele (P2-F: 5′-AAGCAGGGCTGGAGGTAGTC-3′ and P2-R: 5′-TTCTCCCTCTGCCCTACATTC-3′). All breeding and animal procedures were carried out according to institutional regulations of the Rhode Island Hospital animal facility (IACUC protocol no. 0221-06).

Northern blotting

Total RNA was isolated from primary cultured MEFs using TRI Reagent (Molecular Research Center, Cincinnati, OH, USA), and 30 μg of RNA was resolved on 1% agarose gels under denaturing conditions. After transfer to nitrocellulose, blots were hybridized with one of two probes labeled with [^{32}P] deoxy-CTP by random priming (Multiple DNA Labeling Kit, Amersham, GE Healthcare-Life Science, Piscataway, NJ, USA). Probe A was generated by amplifying a 450 bp fragment from GIGYF2 cDNA using primers spanning exons 1 to 4 (NT-F: 5′-T T T G G G C C T G A A T G G C T C C G T G C-3′ and NT-R: 5′-C T T C T T G A A G C T G G A G A T C C T C G-3′), thus matching sequence 5′ from the gene trap insertion. Probe B, corresponding to a region downstream from the gene trap vector, was obtained by *Hin*dIII digestion of GIGYF2 cDNA (1738–2769 bp, exons 13–26). Blots were washed twice with 2× SSC-0.05% SDS (40 min each) and once with 0.1× SSC-0.1% SDS, and specific mRNA bands were identified using a PhosphorImager (Molecular Dynamics, Sunnyvale, CA, USA). The GIGYF1 probe for northern blotting was generated by restriction digestion of mouse GIGYF1 cDNA using *Bam*HI–*Xho*I, generating a 450 bp fragment at the N terminus.

Immunoblotting

For total protein lysates, MEFs derived from *Gigyf2*$^{+/+}$ and −/− mice or whole embryos from timed matings, were homogenized in a 1% NP-40 buffer containing 10% glycerol, 137 mM NaCl, 1 mM $MgCl_2$, 1 mM $CaCl_2$, 20 mM Tris–HCl

at pH 7.6, 2 mM EDTA, 10 mM sodium pyrophosphate, 10 mM NaF, 2 mM Na_2VO_4, 2 mM PMSF and protease inhibitors (Sigma, St Louis, MO, USA). For IGF-I stimulation experiments, *Gigyf2*$^{+/+}$ and −/− MEFs were cultured for 6 h in serum-free Dulbecco's modified Eagle's medium (4.5 g/l glucose) supplemented with 0.5% bovine serum albumin and 25 mM HEPES at pH 7.5. Cells were incubated with 10^{-7} M IGF-I (GroPep, Adelaide, Australia) for the indicated duration at 37°C prior to lysis in 1% NP-40 buffer. All lysates were cleared by centrifugation, protein concentrations were determined by Bradford assay, and 50–60 μg protein aliquots were subjected to SDS–PAGE and transferred to nitrocellulose membranes for immunoblotting. Membranes were blocked at room temperature for 1 h with 5% BSA in Tris-buffered saline Tween-20 followed by incubation overnight at 4°C with primary antibody. After washing, membranes were incubated with appropriate secondary antibodies conjugated to horseradish peroxidase (Jackson Immuno Research, West Grove, PA, USA). Immunoblots were developed by Western Lightning Chemiluminescence Reagent Plus (PerkinElmer, Boston, MA, USA), and digital image acquisition was performed on a FluorChem Imaging System (Alpha Innotech, San Leandro, CA, USA). Rabbit anti-mouse GIGYF2 and GIGYF1 polyclonal antibodies for immunoblotting were generated against 17 amino acid peptides corresponding to the C-terminal sequences of these proteins and affinity-purified with the corresponding peptides immobilized on Sulfolink resin (Pierce, Rockford, IL, USA). Addition antibodies included: anti-ERK1 (Transduction Laboratories), anti-Akt (Cell Signaling Technology, Beverly, MA, USA), anti-IGF-I receptor (kindly provided by Dr Kenneth Siddle, Cambridge, UK) and anti-β-actin (C4; Santa Cruz Biotechnology, Santa Cruz, CA, USA); phosphorylation was measured using anti-ACTIVE MAPK (Promega, Madison, WI, USA), anti-phospho-Akt (Thr308) (Cell Signaling Technology) and anti-phospho-IGF-I receptor (pY^{1158}-specific) (BioSource, Camarillo, CA, USA).

Histology and immunohistochemistry

Brain and spinal cord from 15-month-old *Gigyf2*$^{+/+}$ and +/− mouse littermates were fixed overnight in 4% paraformaldehyde/PBS at 4°C, dehydrated with increasing concentrations of ethanol, embedded in paraffin and sectioned sagittally (7–10 μm). Luxol Fast Blue/Hematoxylin&Eosin staining was performed using standard methods. Adjacent sections were rehydrated, treated with Avidin–Biotin blocking solution (Vector Laboratories, Burlingame, CA, USA) and incubated overnight at 4°C in a humidified chamber with sheep anti-α-synuclein antibody (Chemicon, Temecula, CA, USA). Primary antibody detection was performed with biotinylated goat anti-sheep IgG and Vector Elite ABC Reagent (Vector Laboratories). Sections were counterstained with Hematoxylin.

β-Galactosidase staining

Day 14.5 embryos from timed matings were obtained by Caesarean section, washed in PBS, fixed in fresh 2% paraformaldehyde/PBS for 1 h at 4°C, hemisected, fixed for an additional hour and then placed in 18% sucrose overnight at 4°C. Brains from adult *Gigyf2*$^{-/-}$ mice were also treated in a similar manner. After removal of sucrose by blotting, the specimens were equilibrated in OCT (Tissuetech, EMS, Hatfield, PA, USA), positioned in a plastic base mold filled with OCT and frozen. Sagittal sections (10 μm) were prepared, adhered to slides, washed in PBS and incubated for 24 h at 30°C in the dark in fresh X-Gal solution (1 mg/ml X-Gal, 35 mM potassium ferrocyanide, 35 mM potassium ferricyanide, 2 mM $MgCl_2$, 0.02% NP-40 in PBS). After washing in double-distilled water, the sections were counterstained for 2 min with Vector Fast Red (Vector Laboratories), dehydrated and mounted under coverslips.

Motor function studies

A horizontal rotating rod system was used to measure animal balance and coordination (37). Mice were tested at 12–15 months of age. Each animal was housed in a single cage and all experiments were performed during the light phase of a 12:12 h light:dark cycle. Animals were first conditioned on a stationary rod for 1 min and during this time any animal that fell was placed back on the rod. The next day, animals were conditioned at a constant speed of 5 r.p.m. for 90 s. If an animal fell during this time they were placed back on the rod until the end of the conditioning time (38). After conditioning, animals were subjected to one trial per day at 5 r.p.m. for 6 days, for a total of six trials. The length of time each mouse remained on the rod was recorded.

Cell cycle analysis

Gigyf2$^{+/+}$ and −/− primary MEFs (passage 4) were plated onto 10 cm tissue culture plates at 1.5×10^6 cells/plate and cultured for 24 h in Dulbecco's modified Eagle's medium (4.5 g/l glucose) supplemented with 10% fetal bovine serum. Cells were incubated with 20 μM Etoposide (Sigma) dissolved in DMSO or DMSO alone for an additional 24 h prior to staining with propidium iodide and cell cycle analysis by flow cytometry.

Statistical analysis

Statistical analysis was conducted using Sigma Stat 3.0 and Sigma Plot software (Systat Software, San Jose, CA, USA). One-tailed or two-tailed *t*-tests and the Mann–Whitney rank sum test were performed as indicated to evaluate the significance of differences between means. Results with $P < 0.05$ were considered to be statistically significant.

Conflict of Interest statement. None declared.

FUNDING

Portions of this work were supported by the COBRE Genomics Center at Brown University (J.K.), the Hallett Center for Diabetes and Endocrinology at Rhode Island Hospital (R.J.S.) and NIH Grant DK43038 (R.J.S.).

REFERENCES

1. Giovannone, B., Lee, E., Laviola, L., Giorgino, F., Cleveland, K.A. and Smith, R.J. (2003) Two novel proteins that are linked to insulin-like growth factor (IGF-I) receptors by the Grb10 adapter and modulate IGF-I signaling. *J. Biol. Chem.*, **278**, 31564–31573.
2. Holt, L.J. and Siddle, K. (2005) Grb10 and Grb14: enigmatic regulators of insulin action–and more? *Biochem. J.*, **388**, 393–406.
3. Langlais, P., Dong, L.Q., Ramos, F.J., Hu, D., Li, Y., Quon, M.J. and Liu, F. (2004) Negative regulation of insulin-stimulated mitogen-activated protein kinase signaling by Grb10. *Mol. Endocrinol.*, **18**, 350–358.
4. Dufresne, A.M. and Smith, R.J. (2005) The adapter protein GRB10 is an endogenous negative regulator of insulin-like growth factor signaling. *Endocrinology*, **146**, 4399–4409.
5. Pankratz, N., Nichols, W.C., Uniacke, S.K., Halter, C., Rudolph, A., Shults, C., Conneally, P.M. and Foroud, T. (2002) Genome screen to identify susceptibility genes for Parkinson disease in a sample without parkin mutations. *Am. J. Hum. Genet.*, **71**, 124–135.
6. Trejo, J.L., Carro, E., Garcia-Galloway, E. and Torres-Alemann, I. (2004) Role of insulin-like growth factor I signaling in neurodegenerative diseases. *J. Mol. Med.*, **82**, 156–162.
7. Craft, S. and Wastson, G.S. (2004) Insulin and neurodegenerative disease: shared and specific mechanisms. *Lancet Neurol.*, **3**, 169–178.
8. Russo, V.C., Gluckman, P.D., Feldman, E.L. and Werther, G.A. (2005) The insulin-like growth factor system and its pleiotropic functions in brain. *Endo. Rev.*, **26**, 916–943.
9. Offen, D., Shtaif, B., Hadad, D., Weizman, A., Melamed, E. and Gil-Ad, I. (2001) Protective effect of insulin-like-growth-factor-1 against dopamine-induced neurotoxicity in human and rodent neuronal cultures: possible implications for Parkinson's disease. *Neurosci. Lett.*, **316**, 129–132.
10. Moroo, I., Yamada, T., Makino, H., Tooyama, I., McGeer, P.L. and Hirayama, K. (1994) Loss of insulin receptor immunoreactivity from the substantia nigra pars compacta neurons in Parkinson's disease. *Acta Neuropathol. (Berl)*, **87**, 343–348.
11. Hu, G., Jousilahti, P., Bidel, S., Antikainen, R. and Tuomilehto, J. (2007) Type 2 diabetes and the risk of Parkinson's disease. *Diabetes Care*, **30**, 842–847.
12. Lautier, C., Goldwurm, S., Dürr, A., Giovannone, B., Tsiaras, W.G., Pezzoli, G., Brice, A. and Smith, R.J. (2008) Mutations in the *GIGYF2 (TNRC15)* Gene at the PARK11 locus in familial Parkinson's disease. *Am. J. Hum. Genet.*, **82**, 822–833.
13. Tan, E.K., Lin, C.H., Tai, C.H., Tan, L.C., Chen, M.L., Li, R., Lim, H.Q., Pavanni, R., Yuen, Y., Prakash, K.M. *et al.* (2009) Non-synonymous GIGYF2 variants in Parkinson's disease from two Asian populations. *Hum. Gen.*, [Epub ahead of print, 16 May 2009].
14. Bras, J., Simon-Sanchez, J., Federoff, M., Morgadinho, A., Januario, C., Ribeiro, M., Cunha, L., Oliveira, C. and Singleton, A.B. (2009) Lack of replication of association between *GIGYF2* variants and Parkinson disease. *Hum. Mol. Genet.*, **18**, 341–346.
15. Vilarino-Guell, C., Ross, O.A., Soto, A.I., Farrer, M.J., Haugarvoll, K., Aasly, J.O., Uitti, R.J. and Wszolek, Z.K. (2009) Reported mutations in GIGYF2 are not a common cause of Parkinson's disease. *Mov. Disord.*, **24**, 618–619.
16. Sutherland, G.T., Siebert, G.A., Newman, J.R., Silburn, P.A., Boyle, R.S., O'Sullivan, J.D. and Mellick, G.D. (2009) Haplotype analysis of the Park11 gene, GIGYF2, in sporadic Parkinson's disease. *Mov. Disord.*, **24**, 449–452.
17. Zimprich, A., Schulte, C., Reinthaler, E., Haubenberger, D., Balzar, J., Lichtner, P., El Tawil, S., Edris, S., Foki, T., Pirker, W. *et al.* (2009) PARK11 gene (GIGYF2) variants Asn56Ser and Asn457Thr are not pathogenic for Parkinson's disease. *Parkinsonism Relat. Disord.*, [Epub ahead of print, 26 February 2009].
18. Di Fonzo, A., Fabrizio, E., Thomas, A., Fincati, E., Marconi, R., Tinazzi, M., Breedveld, G.J., Simons, E.J., Chien, H.F., Ferreira, J.J. *et al.* (2009) GIGYF2 mutations are not a frequent cause of familial Parkinson's disease. *Parkinsonism Relat. Disord.*, [Epub ahead of print, 30 May 2009].
19. Meeus, B., Nuytemans, K., Crosiers, D., Engelborghs, S., Pals, P., Pickut, B., Peeters, K., Mattheijssens, M., Corsmit, E., Cras, P. *et al.* (2009) GIGYF2 has no major role in Parkinson genetic etiology in a Belgian population. *Neurobiol. Aging*, [Epub ahead of print, 23 March 2009].
20. Nichols, W.C., Kissell, D.K., Pankratz, N., Pauciulo, M.W., Elsaesser, V.E., Clark, K.A., Halter, C.A., Rudolph, A., Wojcieszek, J., Pfeiffer, R.F. and Foroud, T. for the Parkinson Study Group—PROGENI Investigators (2009) Variation in GIGYF2 is not associated with Parkinson disease. *Neurology*, **72**, 1886–1892.
21. Bonifati, V. (2009) Is *GIGYF2* the defective gene at the PARK11 locus? *Curr. Neuro. Neurosci. Rep.*, **9**, 185–187.
22. Wang, S.S., Lewcock, J.W., Feinstein, P., Mombaerts, P. and Reed, R.R. (2004) Genetic disruptions of *O/E2* and *O/E3* genes reveal involvement in olfactory receptor neuron projection. *Development*, **131**, 1377–1388.
23. Parrish, M., Ott, T., Lance-Jones, C., Schuetz, G., Schwaeger-Nickolenko, A. and Monaghan, A.P. (2004) Loss of the *Sall3* gene leads to palate deficiency, abnormalities in cranial nerves, and perinatal lethality. *Mol. Cell Biol.*, **24**, 7102–7112.
24. Scolnick, J.A., Cui, K., Duggan, C.D., Xuan, S., Yuan, X.B., Efstratiadis, A. and Ngai, J. (2008) Role of IGF signaling in olfactory sensory map formation and axon guidance. *Neuron*, **57**, 847–857.
25. Hawkes, C. (2003) Olfaction in neurodegenerative disorders. *Mov. Disord*, **18**, 364–372.
26. Belluscio, L., Gold, G.H., Nemes, A. and Axel, R. (1998) Mice deficient in G_{olf} are anosmic. *Neuron*, **20**, 69–81.
27. Goldberg, M.S., Fleming, S.M., Palacino, J.L., Cepeda, C., Lam, H.A., Bhatnagar, A., Meloni, E.G., Wu, N., Ackerson, L.C., Klapstein, G.J. *et al.* (2003) Parkin-deficient mice exhibit nigrostriatal deficits but not loss of dopaminergic neurons. *J. Biol. Chem.*, **278**, 43628–43635.
28. Goldberg, M.S., Pisani, A., Haburcak, M., Vortherms, T.A., Kitada, T., Costa, C., Tong, Y., Martella, G., Tscherter, A., Martins, A. *et al.* (2005) Nigrostriatal dopaminergic deficits and hypokinesia caused by inactivation of the familial Parkinsonism-linked gene DJ-1. *Neuron*, **45**, 489–496.
29. Kim, R.H., Smith, P.D., Aleyasin, H., Hayley, S., Mount, M.P., Pownall, S., Wakeham, A., You-Ten, A.J., Kalia, S.K., Horne, P. *et al.* (2005) Hypersensitivity of DJ-1-deficient mice to 1-methyl-4-phenyl-1,2,3,6-tetrahydropyrindine (MPTP) and oxidative stress. *Proc. Natl Acad. Sci. USA*, **102**, 5215–5220.
30. Thiruchelvam, M.J., Powers, J.M., Cory-Slechta, D.A. and Richfield, E.K. (2004) Risk factors for dopaminergic neuron loss in human α-synuclein transgenic mice. *Eur. J. Neurosci.*, **19**, 845–854.
31. Scheele, C., Nielsen, A.R., Walden, T.B., Sewell, D.A., Fischer, C.P., Brogan, R.J., Petrovic, N., Larsson, O., Tesch, P.A., Wennmalm, K. *et al.* (2007) Altered regulation of the PINK1 locus: a link between type 2 diabetes and neurodegeneration. *FASEB J.*, **21**, 3653–3665.
32. de la Monte S.M. and Wands J.R (2005) Review of insulin and insulin-like growth factor expression, signaling, and malfunction in the central nervous system: relevance to Alzheimer's disease. *J. Alzheim. Dis.*, **7**, 45–61.
33. Carson, M.J., Behringer, R.R., Brinster, R.L. and McMorris, F.A. (1993) Insulin-like growth factor I increases brain growth and central nervous system myelination in transgenic mice. *Neuron*, **10**, 729–740.
34. Unger, J.W., Livingston, J.N. and Moss, A.M. (1991) Insulin receptors in the central nervous system: localization, signaling, mechanisms, and functional aspects. *Prog. Neurobiol.*, **36**, 343–362.
35. Irie, F., Fitzpatrick, A.L., Lopez, O.L., Kuller, L.H., Peila, R., Newman, A.B. and Launer, L.J. (2008) Enhanced risk for Alzheimer disease in persons with type 2 diabetes and APOE epsilon4: the cardiovascular health study cognition study. *Arch. Neurol.*, **65**, 89–93.
36. Xu, W.L., von Strauss, E., Qiu, C.X., Winblad, B. and Fratiglioni, L. (2009) Uncontrolled diabetes increases the risk of Alzheimer's disease: a population-based cohort study. *Diabetologia*, **52**, 1031–1039.
37. Brooks, S.P., Pask, T., Jones, L. and Dunnett, S.B. (2004) Behavioral profiles of inbred mosue strains used as transgenic backgrounds. I. Motor tests. *Genes Brain Behav.*, **3**, 206–215.
38. Jiang, C., Wan, X., He, Y., Pan, T., Jankovic, J. and Le, W. (2005) Age-dependent dopaminergic dysfunction on Nurr1 knockout mice. *Exp. Neurol.*, **191**, 154–162.